



# Assimilation window in 3D-Var

Prague, 20/06/2014 - 30/07/2014

Patrik Benacek  
Czech Hydrometeorological Institute (CHMI),  
Na Sabatce 17, 143 06 Prague 4, Czech Republic

# Contents

<b>1</b>	<b>Introduction</b>	<b>3</b>
<b>2</b>	<b>Data and Methodology</b>	<b>3</b>
2.1	Model and 3D-Var system . . . . .	3
2.2	Polar satellite data . . . . .	5
<b>3</b>	<b>Results</b>	<b>7</b>
3.1	Data coverage . . . . .	7
3.2	Non-stationary condition . . . . .	8
3.2.1	MRH channels . . . . .	10
3.2.2	HT channels . . . . .	11
3.2.3	LT channels . . . . .	12
3.2.4	MT channels . . . . .	13
3.3	Sensor IASI . . . . .	14
3.3.1	Cloud detection scheme . . . . .	14
3.4	Long-Time assessment . . . . .	16
3.5	Optimal assimilation window . . . . .	17
<b>4</b>	<b>Conclusion</b>	<b>20</b>
<b>A</b>	<b>Cloud detection scheme</b>	<b>22</b>

# 1 Introduction

This work assesses impact of assimilating polar satellite observation on weather prediction using the three-dimensional variational data assimilation (3D-Var) and forecasting system of the ALADIN (Aire Limitee Adaptation dynamique Developpement InterNational) model. The assimilation scheme is based on a 6h-assimilation window supposing a stationary model first guess within this time-window. A time-delay parameter representing difference between observation and analysis time is changed to assess a representativeness of data within the assimilation window for different type of instruments: AMSU-A (the Advanced Microwave Sounding Unit-A), MHS (the Microwave Humidity Sounder) and IASI (the Infrared Atmospheric Sounding Interferometer) on board of polar satellites.

## 2 Data and Methodology

### 2.1 Model and 3D-Var system

We will use a hydrostatic version of limited area model ALADIN (Aire Limitee Adaptation dynamique Developpement InterNational) for the cycle CY38t1 to perform data assimilation and weather forecast. The model domain covers Middle Europe (2.1W-27.4E, 40.6N-55.7N) with 4.7 km horizontal resolution. The vertical resolution is fixed at 87 unequally spaced vertical levels covering the troposphere and then loosely the stratosphere up to 0.1 hPa. It is coupled every 3 hours with the ARPEGE forecast on its lateral boundaries.

Data assimilation system consists from 3-dimensional variational assimilation scheme 3D-Var (Brousseau et al., 2008). It has an incremental formulation originally introduced in the ARPEGE-IFS global data-assimilation system. The theory and implementation for variational data assimilation in numerical weather prediction are well established in [6]. The optimal atmospheric state,  $x$ , can be found as the one that minimizes the cost function:

$$J(x) = (x_b - x)^T B^{-1} (x_b - x) + (y - H(x))^T R^{-1} \underbrace{(y - H(x))}_{\delta y} \quad (1)$$

where  $x$  is analysis,  $x_b$  is a prior estimation of model state (background, first guess),  $B$  is the background error covariance matrix,  $H(x)$  is the observation operator projected of the model state onto the observation space,  $y$  is the observation and  $R$  is the observation error covariance matrix. Differences between observations and model equivalent are called *observation increments*  $\delta y$  and provide information about a contribution of measurement to analysis.

In our study,  $y$  contains the radiance measurements from instruments on board of polar satellites. The observation operator  $H(x)$  allows to assimilate radiance through the Radiative Transfer for TOVS (RTTOV) model (Saunders et al., 1999), one of the latest version RTTOV-9 recently developed within the EUMETSAT NWP Satellite Application Facility (SAF) will be used. The observation error covariance matrix is assumed to be diagonal simplifying the implementation of data assimilation equation and improving computational efficiency. Finally, the background error covariance matrix was generated by the ensemble method described in [1].

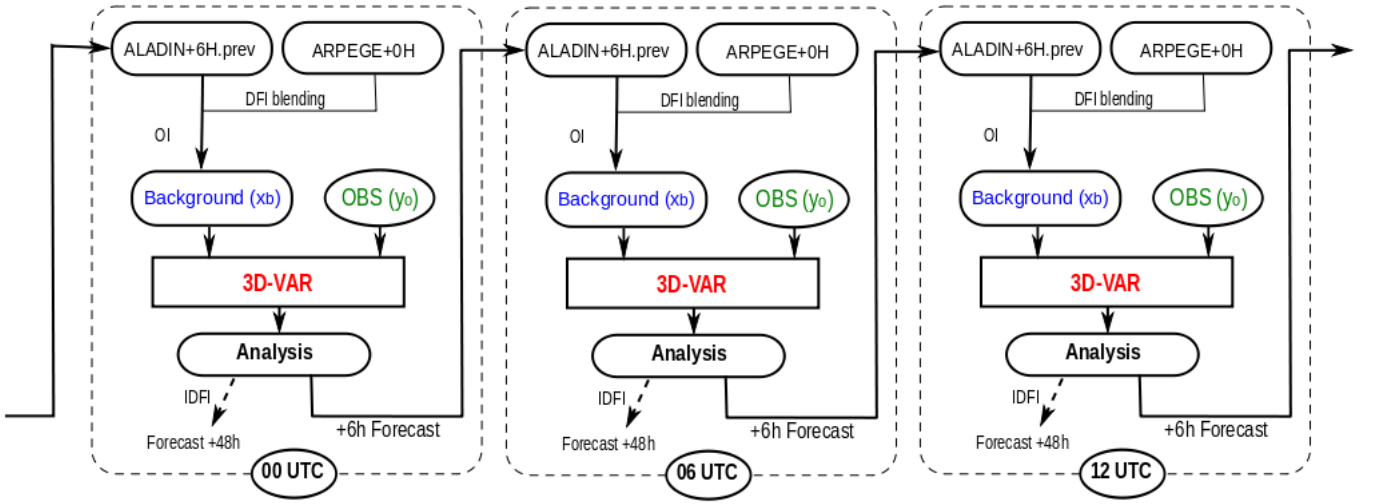


Figure 1: Data assimilation system scheme in model ALADIN/CZ.

The assimilation system uses a six-hour forward intermittent cycle as is shown in Fig 1. A six-hour forecast (*ALADIN + 6H.prev*) from a previous cycle is used as a first guess. This guess is blended with the global Arpege analysis (*ARPEGE + 0H*) using ALADIN blending technique described in [2]. On the top of the blending problem is performed a surface data assimilation by optimal interpolation method (OI, [5]). The resulting background field is analyzed with observation in the 3D-Var assimilation system. A six-hour forecast is run from analysis and used in the next assimilation cycle as first guess. Data assimilation scheme is performed at 00, 06, 12 and 18 UTC and the analyzed fields are two components of the wind, temperature, specific humidity and surface pressure. The other model fields are cycled from the previous ALADIN guess.

### Assimilation window

The 3D-Var algorithm is a simplification of the full variational data assimilation scheme, making the assumption that model field is stationary within a wide time-range called *assimilation window*. In that case, the observation within the window although depending on time, are considered as observation of the analysis time. This scheme is shown in Fig 2.

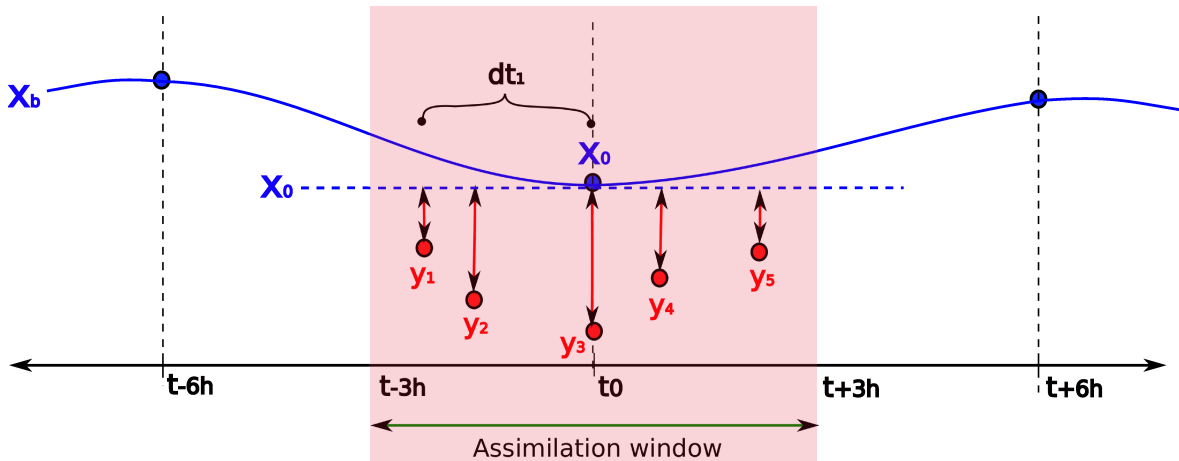


Figure 2: The scheme of 6h-assimilation window using in the 3D-Var system.

Note that observation  $y_i$  measured at times  $t_i$  are collected within the assimilation window (red field) and compared with the model background  $x_0$  at the analysis time  $t_0$ . This suppose that the model background is stationary within the assimilation time-window and observation increments

are computed as  $\delta y_i = y_i - H(x_0)$ . However, in case of non-stationary weather conditions, the difference between  $x_b$  and  $x_0$  have not to be negligible and could lead to increasing of observation increment error. This error depends on a time-delay  $\delta t$  between measurements and analysis time. The higher time-delay the higher observation increment error. This effect is described as a non-stationary conditions problem and depends on a length of assimilation window, weather conditions and measured quantities.

The length of assimilation window is usually set in 3D-Var assimilation system according to a type of observation. Conventional observations (e.g. synoptic stations, radiosondes, wind-profilers) as well as geostationary satellites provide measurements at analysis time. Aircraft observations are analyzed within 3h-assimilation window, whereas polar satellites are analyzed within 6h-assimilation window.

The weather conditions could contribute to the non-stationary problem. The unstable atmosphere is subject to a high degree of variability through distance and time. This conditions could increase the difference between model background and analysis state within the assimilation window manifesting by displacements between clouds, humidity or temperature features.

The effect of non-stationary conditions depends also on measured quantities. The quantities which are sensitive to atmosphere variability (e.g. humidity, clouds, surface temperature) could be more affected by the time-delay within the assimilation window. This involves polar satellite instruments sensitive to atmospheric humidity/clouds or temperature-sensitive instruments with low-peaking channels.

## 2.2 Polar satellite data

Polar orbiting satellites are an important class of meteorological and geophysical satellite. Typically, these satellites are placed in circular sun-synchronous orbits. Their altitudes usually range from 700 to 800 km, with orbital periods of 98 to 102 minutes. The lower Earth orbits is better positioned to obtain high quality remote-sensing data with a scan swath of the satellite's instrumentation about 3000 km. Satellites in this category include the NOAA Polar-orbiting Operational Environmental Satellites (POES) and Met-Op satellites. They provide together continuous data over Europe.

The satellite-borne instruments measure radiance emitted from the system Earth/atmosphere at visible (VIS), infrared (IR) or microwave (MW) frequencies. Following instruments on board of polar satellites are used in this study:

**IASI** – the Infrared Atmospheric Sounding Interferometer is an instrument on board of MetOp-A (launched in 2006) and MetOp-B (2012). This instrument measures the Earth emitted IR radiance between  $3.5 - 18\mu m$  with very high spectral resolution (8461 channels). It provides performance for measuring atmospheric temperature and humidity profiles. This measurements are often contaminated by clouds. The current assimilation systems are not able to make use of cloud-contaminated radiances, therefore cloud-detection schemes providing cloud cleaning must be applied [8], [7]. The ground resolution of scanner is 12 km IFOV (the Instantaneous Field of View).

**AMSU-A** – the Advanced Microwave Sounding Unit-A is an instrument on board of NOAA, MetOp and EOS satellites. This instrument is capable of retrieving vertical temperature profiles of the atmosphere using 15 channels including the 54 GHz band. The measurements are with coarser vertical resolution, however, the clouds generally have a very small effect with the exception of precipitation. The precipitation is pre-calculated from observed brightness temperature of surface sensitive channel 1, 2, 3 and 15. The ground resolution of scanner is 48 km IFOV.

**MHS** – the Microwave Humidity Sounding is instrument on board of e.g. NOAA18, 19 and MetOp satellites. This instrument provides humidity sounding in almost all-weather conditions (also

precipitation) using 5 channels including the 183 GHz band. The ground resolution of scanner is 16 km IFOV.

### 3 Results

The purpose of this work is to assess an effect of 6h-assimilation window on polar satellite data assimilation in case of non-stationary weather conditions. Firstly, we investigate a data coverage over the domain and mean time-delay for each polar satellite in the Sec 3.1. The effect of non-stationary weather conditions on observation increment error is studied for two-different time-delays in Sec 3.2. Furthermore, we investigate this effect for different instruments/channels to understand the error dependency on different measured quantities. Time-delay effect for all-sky conditions is studied by monitoring of increment errors for long-time period in Sec 3.4. Finally, we investigate an optimal length of assimilation window for each satellite instrument in Sec 3.5. This is based on assessing the dependency between time-delay and observation increment error for long-time period.

#### 3.1 Data coverage

We investigate a polar satellite’s data coverage over the domain during a period 3.-30.9.2013. A distribution of collected data over the period (normalized against maximum value) is shown for NOAA-18, NOAA-19, MetOp-A and MetOp-B in Fig 3. Note that all polar satellites cross the domain twice/day. Satellites NOAA-18 and NOAA-19 have orbits very close to each other as well as MetOp-A and MetOp-B. The MetOp satellites are shifted about 30 minutes from each other, whereas the NOAA satellites are shifted about 2 hours from each other.

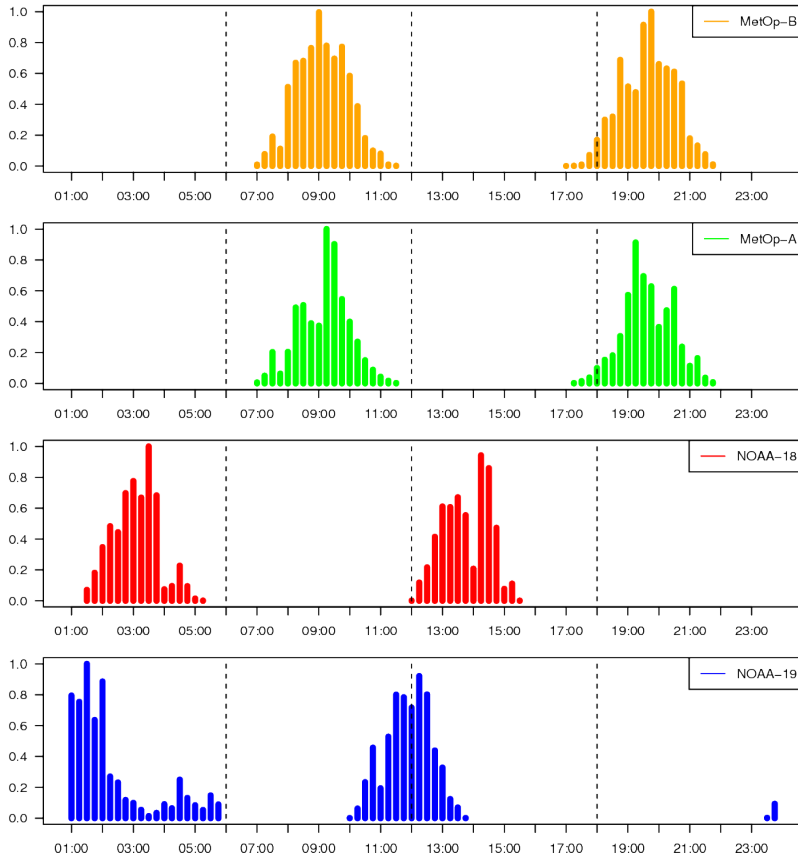


Figure 3: ATOVS satellite crossing times across ALADIN/CZ domain.

Data are assimilated into the model every 6 hour at analysis times 0, 6, 12 and 18 UTC. Note that satellites MetOp-A, B and NOAA-18 provide most of measurements outside the analysis times, except of NOAA-19 providing measurements close to analysis times 0 and 12 UTC. Time delays  $\delta t$  between the analysis and observations are described for each satellite in Tab 1. Note that almost all polar

satellites provide measurements delayed above 2-3 hours from analysis time. The 6h-assimilation window is able to collect all the data and increase an assimilation data sample.

Table 1: Mean time-delays  $\delta t$  of polar satellites.

Satellite	$\delta t$ [h]
NOAA-18	2-3
NOAA-19	0-1
MetOp-A, B	2-3

### 3.2 Non-stationary condition

The satellite data  $y$  are passively assimilated<sup>1</sup> to the model at analysis time  $t_1$  and  $t_2$  to simulate different time-delays  $\delta t_1$  and  $\delta t_2$ . Then we expressed observation increments  $\delta y_1$  and  $\delta y_2$  corresponding to the time-delays as:

$$\begin{aligned}\delta y_1 &= y - H(x_1) \\ \delta y_2 &= y - H(x_2)\end{aligned}$$

where  $x_1$  and  $x_2$  are first-guesses at the times  $t_1$  and  $t_2$ . The observation increments  $\delta y$  are investigated depending on time-delays  $\delta t$  for each satellite's instrument.

The effect of non-stationary weather conditions on 3.9.2013 is investigated in this study. We use data from polar satellite MetOp-B measured over the domain at 9:20 UTC. These data are analyzed at  $t_1 = 9$  UTC and  $t_2 = 12$  UTC to study corresponding time-delays  $\delta t_1 = 20$  min and  $\delta t_2 = 160$  min. The observation increments are studied depending on time-delays  $\delta t$  for each sensor AMSU-A, MHS and IASI on board of the satellite. Sensors measure radiances at spectral channels providing information about atmospheric temperature/humidity at different altitudes. We select channels separately according their altitude sensitivity and spectral range. The list of studied channels is described in Tab 2.

Table 2: List of selected sensors/channels on board of MetOp-B used in this study.

Sensor(channels)	Sensitivity range	Category
AMSU-A (8,9) IASI (212-269)	200-300hPa	High-tropospheric temperature channels (HT)
AMSU-A (6,7) IASI (271-306)	300-500hPa	Middle-tropospheric temperature channels (MT)
AMSU-A (5) IASI (308-457)	500-1000hPa	Low-tropospheric temperature channels (LT)
IASI (580-1341)	surface	Surface temperature channels (ST)
MHS (3,4) IASI (2701,3027)	400-600hPa	Middle-tropospheric humidity channels (MRH)

<sup>1</sup>Passive assimilation method allows to process data through 3D-Var system, however, the data have any effect on analysis improvement. Supposing that the resulting analysis is the same as initial model first-guess we will called the assessed observation-minus-guess departures as observation increments.

## Weather situation

This investigation is performed for non-stationary weather conditions on 3.9.2013. Central Europe is affected by an extra-tropical cyclone centered in North Ukraine as is shown from VIS-IR product in the top Fig 4. This cyclone affects Central Europe by frontal cloud band (over Germany, Czech Republic and Hungary). Behind this cold frontal line is strong advection of cold dry air from north-west detected in VIS-IR as a clear-sky wedge over Poland. The point of the occlusion is situated on the Slovakia-Ukraine border. There is a strong warm advection as well as in the whole cloudiness of the occlusion. West Europe is affected by high pressure with a stationary clear-sky weather. The synoptic map with marked frontal lines is shown in the bottom Fig 4.

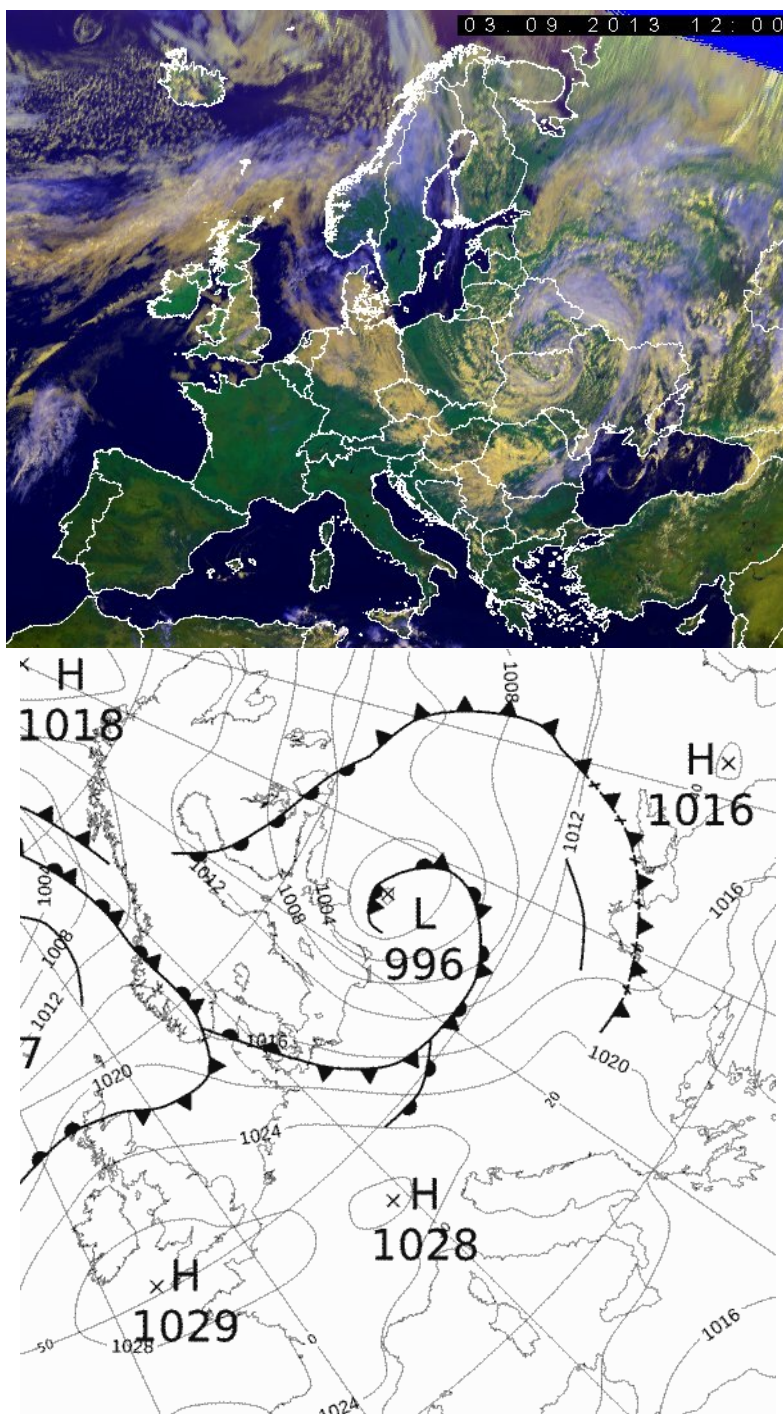


Figure 4: Combination of MSG VIS-IR channels (top) and synoptic map over Europe (bottom) from 3.9.2013 at 12 UTC. Sources are CHMI-Libus and MetOffice.gov.uk.

## Smooth fields

We study a displacement of atmospheric features detected between model first guess (FG) at times  $t_1$  and  $t_2$  and satellite observations. Satellite measurements  $y$  and model equivalent  $H(x)$  are available in a spatially irregular observation space. To study features, the set of irregular data is interpolated to 2-dimensional grid point fields that are smoothed using Gaussian kernel smoothing method (more details in R-package `spatstat` description). The smoothed fields provide information about spatially distribution of measured radiances and model equivalents. We reduce the model domain to smaller subdomain to avoid increasing interpolation/smoothing errors due to insufficient data coverage.

Observation increment field is get as a difference between smoothed FG and observation field. The blue color represents cold/wet bias resulting from measurements, whereas the red color represents warm/dry bias.

### 3.2.1 MRH channels

We study observation increments for middle-tropospheric humidity channels (MRH) depending on time-delays  $\delta t_1 = 20$  min and  $\delta t_2 = 160$  min. The list of studied sensors/channels and their sensitivity range is in Tab 2.

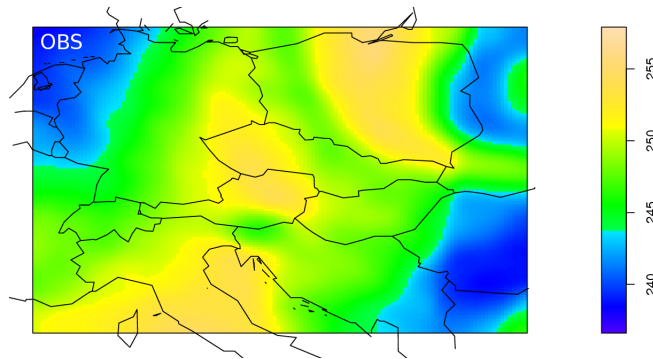


Figure 5: The smoothed observation field for sensor MHS/channel-3 on board of MetOp-B measured at 9:20 UTC.

The smoothed observation field is for sensor MHS/channel-3 shown in Fig 5. The blue features represent humid, cloudy areas, whereas the yellow features represent drier, clear-sky areas both between 400-600hPa. Note that the air-mass in frontal cloud band is characterized by humid, cloud air, whereas there is a wedge of dry-air behind the cold front (over Poland).

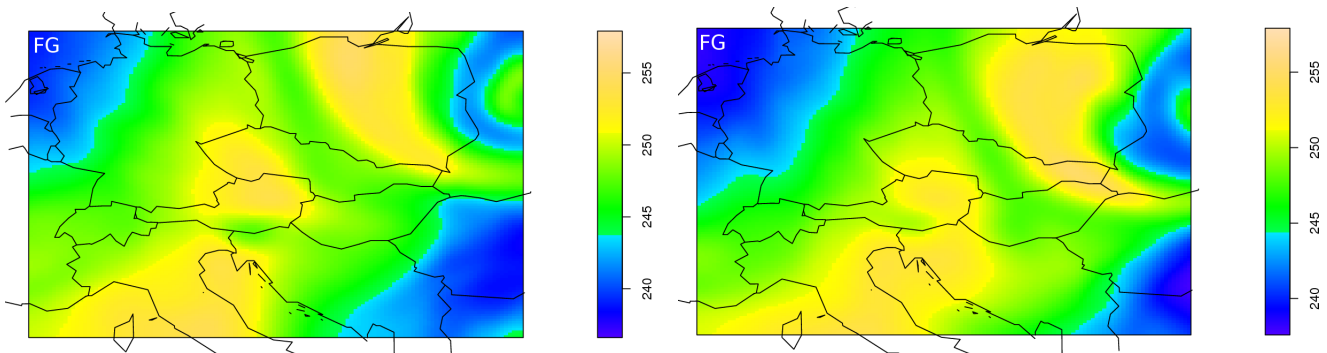


Figure 6: The smoothed FG fields analyzed at time 9 UTC (right) and 12 UTC (left).

The smoothed FG fields analyzed at time 9 UTC and 12 UTC are shown in Fig 6 (left and right). Comparing both model fields note that there is a difference in position of the cold front line. The line moves at 12 UTC about 150 km to the south as well as the wedge of dry-air behind the

line. Despite the fact that we assume the stationary problem within assimilation window, there are obvious differences in middle-troposphere humidity fields.

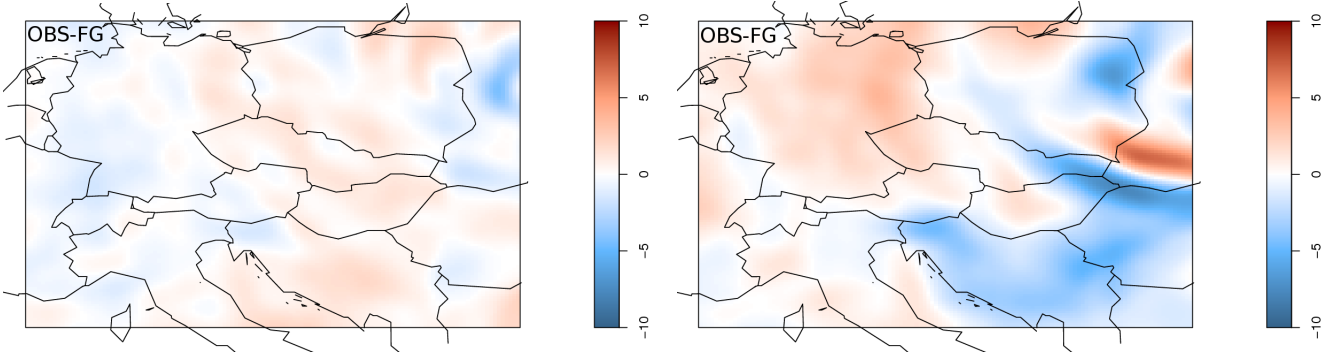


Figure 7: The observation increment fields representing time-delays between observation and model 20 min (left) and 160 min (right).

The impact of non-stationary FG model fields is shown in Fig 7. There are observation increment fields corresponding to time-delays 20 min (left) and 160 min (right). Note that observation increments are in case of 20 min time-delay up to 3 K, however, the longer time-delay between model and observation leads to the higher increments. The increasing of increments is detected for the 160 min time-delay in a vicinity of moving cold-front line (over Slovakia) up to +10 K. Moreover there is obvious that the longer time-delay moisten the analysis instead of drying detected for the shorter delay. This degradation is detected for all studied MRH channels.

### 3.2.2 HT channels

We study observation increments for high-tropospheric temperature channels (HT) depending on time-delays  $\delta t_1 = 20$  min and  $\delta t_2 = 160$  min. The list of studied sensors/channels and their sensitivity range is in Tab 2.

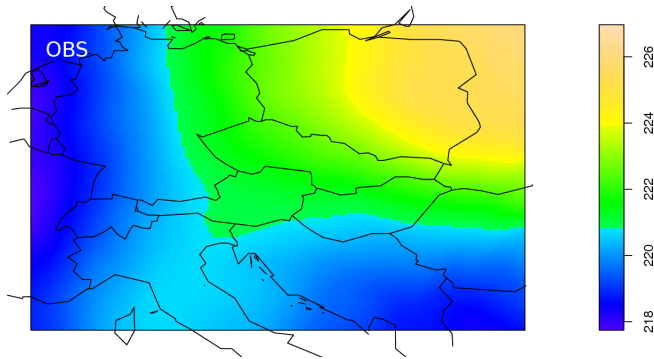


Figure 8: The smoothed observation field for sensor AMSU-A/channel-8 on board of MetOp-B measured at 9:20 UTC.

The smoothed observation field is for sensor AMSU-A/channel-8 shown in Fig 8. The yellow/blue features represent warm/cold layers between 200-300hPa. The observation field indicates cold high-tropospheric air-mass over the whole Europe except of the north-east part, where the warmer air has been lifted in the occluded front.

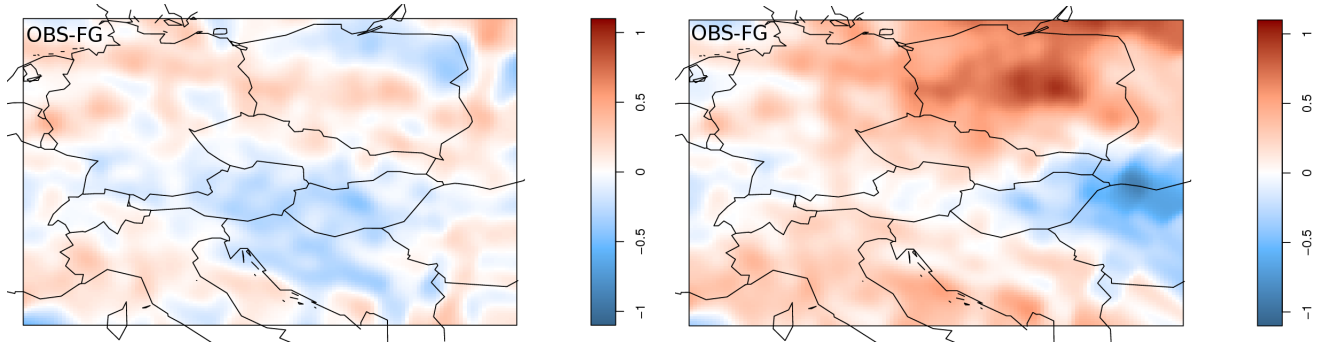


Figure 9: The observation increment fields representing time-delays between observation and model 20 min (left) and 160 min (right).

The impact of time-delays data assimilated at 9 UTC and 12 UTC is obvious from observation increment fields shown in Fig 9. There are detected observation increments delayed 20 min (left) and 160 min (right) from analysis. The longer time-delay 160 min leads to increasing bias of increments. The warm bias (over Poland) is related with cold advection behind cold front, whereas the cold-bias (West Ukraine) is related with warm advection maximum close the occlusion point. The degradation due to a non-stationary high-tropospheric temperature field is for HT channels up to 1 K. This degradation is detected for all studied HT channels.

### 3.2.3 LT channels

We study observation increments for low-tropospheric temperature channels (LT) depending on time-delays  $\delta t_1 = 20$  min and  $\delta t_2 = 160$  min. The list of studied sensors/channels and their sensitivity range is described in Tab 2. The LT channels are sensitivity to temperature layers between 500-1000hPa. They are assimilated for MW sensor AMSU-A over sea/land and for IR sensor IASI only over sea surface. We investigate observation increments depending on time-delays for sensor AMSU-A/channel-5.

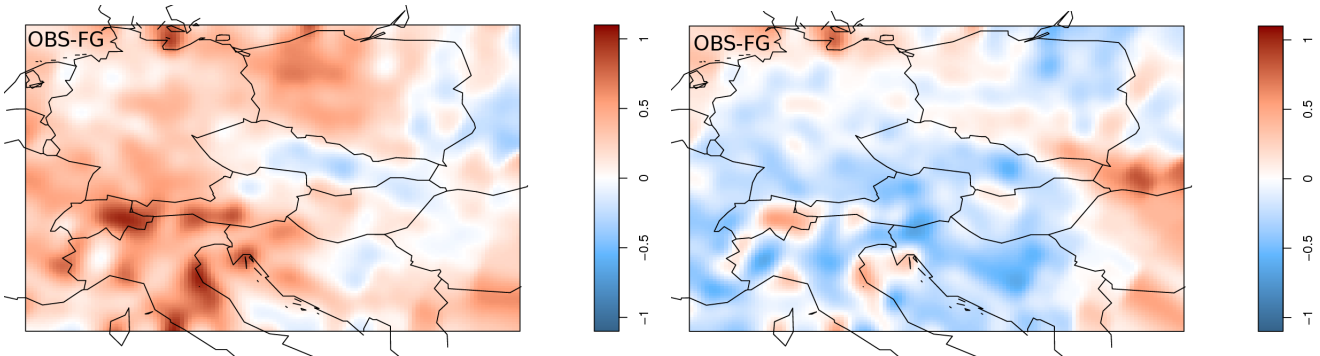


Figure 10: The observation increment fields representing time-delay between observation and model 20 min (left) and 160 min (right).

The impact of time-delays for low-troposphere temperature is shown in Fig 10. There are observation increment fields corresponding to the time-delays 20 min (left) and 160 min (right). Note that the increments are warmer/colder for 20/160 min time-delay over West Europe. This is due to surface heating during a day. At 9 UTC is model first-guess colder than observation (measured 20 min later), however, at 12 UTC is warmer then observation (measured 160 min earlier). The contamination of observation increments by time-delay is for low-tropospheric channels up to 1 K. This degradation is detected for all studied LT channels.

This dependency is much more stronger for the surface temperature (ST) channels (not shown). We assimilate ST channels only for IR sensor IASI over sea surface. This restriction are due to a poor description of surface temperature and surface emissivity by model. For MW sensor AMSU-A are rejected all ST channels due to greater dependence of surface emissivity over sea.

### 3.2.4 MT channels

We study observation increments for middle-tropospheric temperature channels (MT) depending on time-delays  $\delta t_1 = 20$  min and  $\delta t_2 = 160$  min. The list of studied sensors and channels and their sensitivity range is in Tab 2. We investigate observation increments depending on the time-delays for sensor AMSU-A/channel-6. This channel measures a temperature of layer between 300-500hPa.

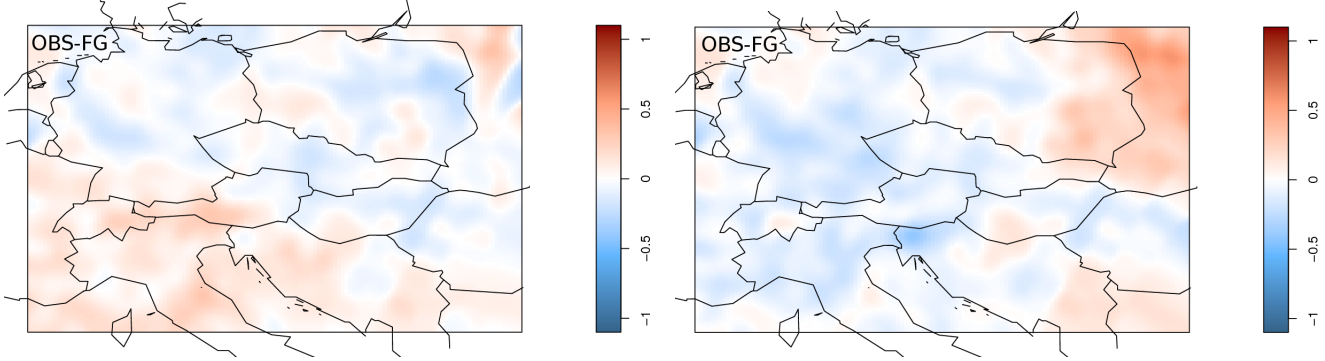


Figure 11: The observation increment fields representing time-delay between observation and model 20 min (left) and 160 min (right).

The smoothed observation increment fields corresponding to time-delays 20min (in left) and 160min (in right) are shown in Fig 11. There is obvious impact of lower-troposphere/surface temperature sensitivity (as is described in Sec 3.2.4) representing by warm/cold bias in West Europe. Furthermore there are also detected warmer increments due to cold advection in North-East Europe as is described for HT channels in Sec 3.2.2. However, note that these degradations of observation increments for the longer time-delay (right) is lower (up to 0.5 K) comparing with the error for HT and ST channels (up to 1 K).

### 3.3 Sensor IASI

This sensor is a hyperspectral sounder measuring brightness temperature (BT) in the infrared (IR) spectral region with 8461 channels. It provides a detailed information about atmospheric temperature and humidity with a high vertical resolution. The measured IR-BT is strongly affected by clouds.

Observation modeling provides a well-established framework for assimilating clear-sky BT data in NWP systems, but there are practical difficulties that limit our ability to make use of cloud-contaminated BT data in a similar manner [4]. Therefore, operational use of BT data in NWP is still mainly restricted to clear channels and cloud-detection schemes must be used to reject the cloud-contaminated data.

#### 3.3.1 Cloud detection scheme

The cloud detection scheme McNally&Watts [8] was used in this study. It is based on looking for radiative effect of a cloud in a curve consisting of vertically-ranked and smoothed FG departures (represented by observation increments). More details could be found in A.

This algorithm works correctly supposing that observation increments are unbiased. Increasing of the time-delays could lead to suboptimal cloud detection and analysis degradation. We aim to investigate a quality of the cloud detection scheme depending on the observation time-delays 20 min and 160 min. A cloudy pixel rejection is investigated for the selected channels described in Tab 2 comparing with CMS (the Cloud Mask Scheme) product available from NWC-SAF ([9]). This product is provided by EUMETSAT and includes information about a cloud coverage and a cloud type over Europe.

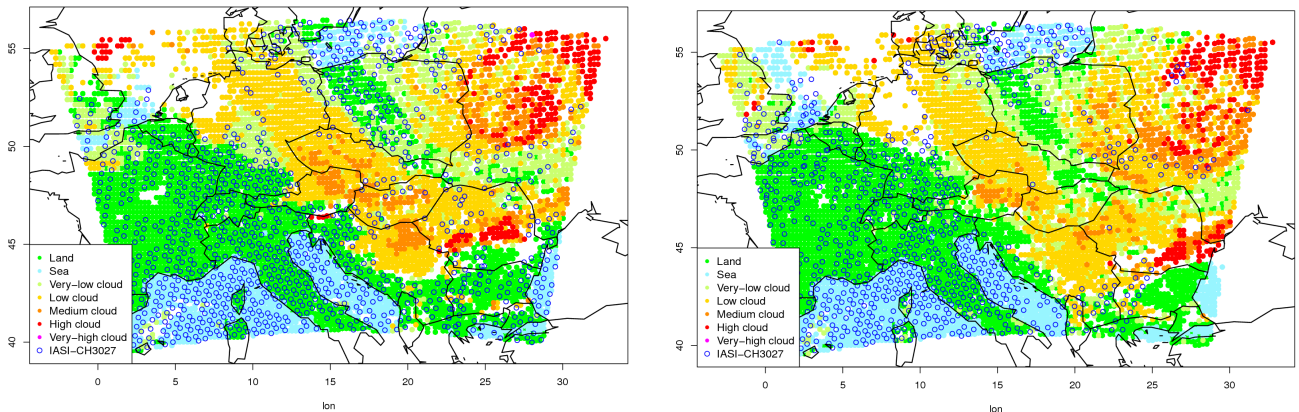


Figure 12: The rejection of cloudy pixels (blue circles) for channel 3027 on board of IASI monitored against CMS products from MSG. The cloud rejection quality is compared between observation time-delays 20 min (left) and 160 min (right).

We detected for all IASI channels that increasing of time-delay (up to 160 min) leads to an inappropriate cloud detection manifesting by incorrect cloud-type detection and data rejection. The CMS information in combination with measurements (after cloudy-pixels rejection) is for MRH channel 3027 and both time delays 20 min (right) and 160 min (left) shown in Fig 12. The measured radiances (blue circles) are sensitive to humidity layer above 500 hPa. The clouds occurring above layer (low, medium, high and very-high clouds) contaminate the measurements and should be rejected. Note that a lot of clear-sky data (green color) are incorrectly rejected for 160 min time-delay. Furthermore, the quality of rejection is degraded for the longer time-delay near the occlusion point (West Ukraine), where the measurements above low-clouds are rejected for 20 min time-delay and wrongly accepted for the 160 min delay.

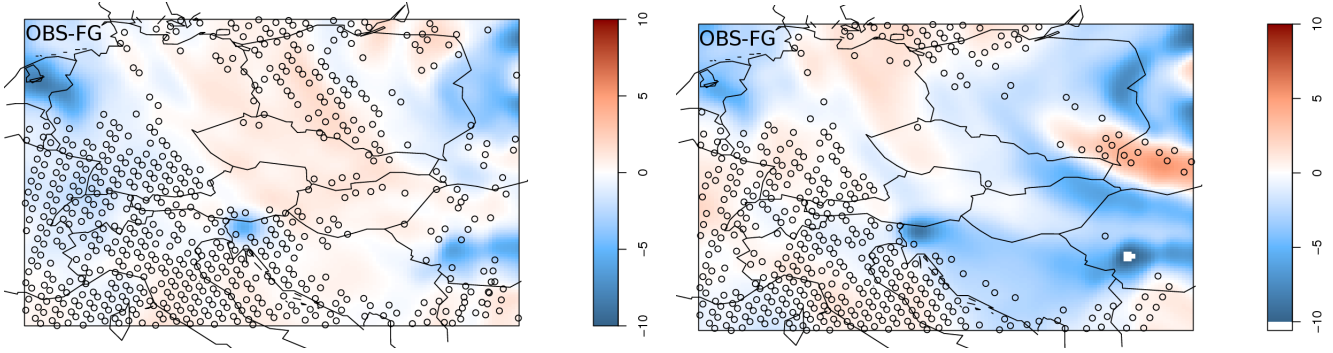


Figure 13: The observation increment fields for MRH channel 3027 in combination with selected data (circles) representing time-delay between observation and model 20 min (left) and 160 min (right).

The smoothed observation increment field in combination with selected pixels is shown for MRH channel 3027 in Fig 13. It provides information about the dependency between selected data and their difference from model first-guess. There are shown the increments for 20 min time-delay (in left) and 160 min (in right). The longer time-delay (right) leads to increasing of increments (up to 10 K) in the region of non-stationary weather conditions (behind the cold front). The colder increments are assessed as cloudy-contaminated and they are rejected. This effect is related with the cloud detection algorithm technique.

This effect is also shown for HT channel 219 in Fig 14 for the time-delays 20 min (in left) and 160 min (in right). This channel is sensitive to high-tropospheric layers between 200-300hPa (similarly as is shown for AMSU-A/channel-8 in Fig 9). Note that the longer time-delay (left) leads to increasing of observation increments in cold/warm advection regions. Cloud detection scheme evaluates incorrectly this situation as cloud-affected and rejects the measurements.

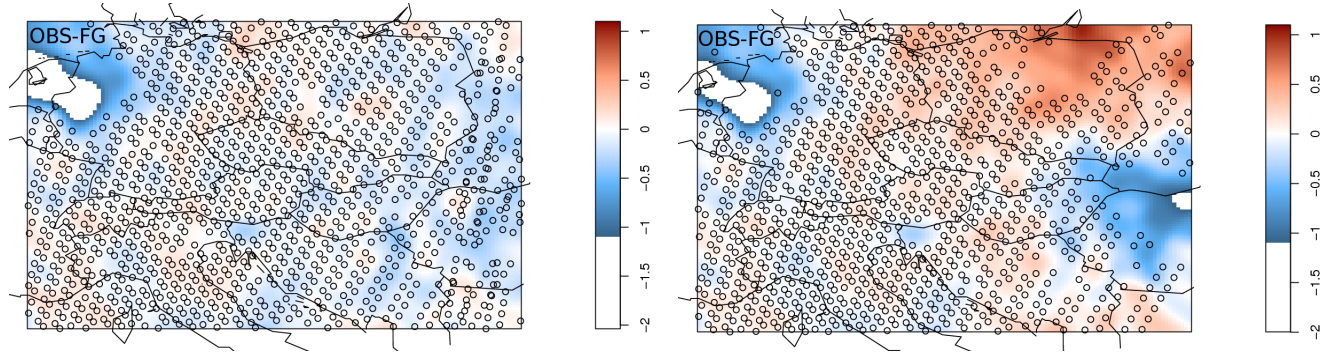


Figure 14: The observation increment fields for HT channel 219 in combination with selected data (circles) representing time-delay between observation and model 20 min (left) and 160 min (right).

### 3.4 Long-Time assessment

An effect of the time-delays is monitored for all weather conditions for a one-month period in 09/2013. We evaluate mean (BIAS) and standard deviation (STD) of observation increments for selected channels/instruments on board of polar satellite MetOp-B described in Tab 2. Data are passively assimilated at 9 and 12 UTC relating with mean time-delays  $\delta t_1 \sim 0$  hour and  $\delta t_2 \sim 3$  hours between first-guess and observations (see in Fig 3).

We apply variational bias correction (VarBC) scheme to correct observation bias. Bias parameters (providing weights to predictors) are used for both assimilated terms from global model ARPEGE available at 12 UTC. Long-time effect of time-delay on satellite data assimilation is described for sensors AMSU-A, MHS and IASI in Tab 3, Tab 4 and Tab 5.

Table 3: The long-time effect of time-delays  $\delta t_1$  and  $\delta t_2$  on sensor AMSU-A.

Channel	BIAS( $\delta t_1$ )	BIAS( $\delta t_2$ )	STD( $\delta t_1$ )	STD( $\delta t_2$ )
5	-0.01	-0.14	0.26	0.26
6	-0.05	-0.09	0.15	0.15
8	0.01	0.04	0.24	0.27
9	-0.02	-0.01	0.18	0.19

Table 4: The long-time effect of time-delays  $\delta t_1$  and  $\delta t_2$  on sensor MHS.

Channel	BIAS( $\delta t_1$ )	BIAS( $\delta t_2$ )	STD( $\delta t_1$ )	STD( $\delta t_2$ )
3	0.03	0.08	1.67	2.20
4	-0.06	0.05	1.48	1.86
5	-0.19	-0.26	1.32	1.47

Table 5: The long-time effect of time-delays  $\delta t_1$  and  $\delta t_2$  on sensor IASI.

Channel	BIAS( $\delta t_1$ )	BIAS( $\delta t_2$ )	STD( $\delta t_1$ )	STD( $\delta t_2$ )
219	-0.02	-0.03	0.29	0.30
269	0.00	-0.06	0.26	0.26
389	0.00	-0.07	0.27	0.27
3027	0.00	0.52	1.28	1.50

The longer time-delay  $\delta t_2$  affects primarily *MRH channels*. The significant degradation of STD and BIAS value is detected for sensors MHS (channels 3-5) and IASI (channel 3027) in Tab 4 and Tab 5. For the *LT/ST channels* is detected increasing BIAS value (for  $\delta t_2$ ) due to surface-temperature sensitivity varying during a day. This is shown for sensor AMSU-A (channel 5) in Tab 3. For the *HT channels* are sensitive to cold/warm advection leading to a small STD degradation for the longer time-delay.

Note that the effect of time-delay is higher for AMSU-A then IASI temperature-sensitive channels. That is due to the cloud-detection scheme for sensor IASI rejecting cold/warm observational increments based on FG departure check. Then the influence of time-delay is assessed as a cloud-contamination and the negative effect is reduced.

### 3.5 Optimal assimilation window

We investigate a dependency between time-delay and observation increment to find an optimal length of the assimilation window in 3D-Var system. This dependency is studied for selected sensors and channels on board of MetOp-B described in Tab 2.

The measurements are passively assimilated at analysis times 0, 6, 9, 12 and 18 UTC to provide a sufficient observation sample. Data analyzed at 0, 6, 12 and 18 UTC are collected within 6h-assimilation window to provide time-delays 1 – 3 hours, whereas data analyzed at 9 UTC are collected within 3h-window to provide time-delays 0 – 1.5 hours. Finally, the dependency between observation increments and the time-delays is monitored to investigate a behavior of observation increment error. To avoid a noise effect, the dependency is fitted using a cubic smoothing spline with smoothing parameter  $spar = 0.5$  (more details in [3]).

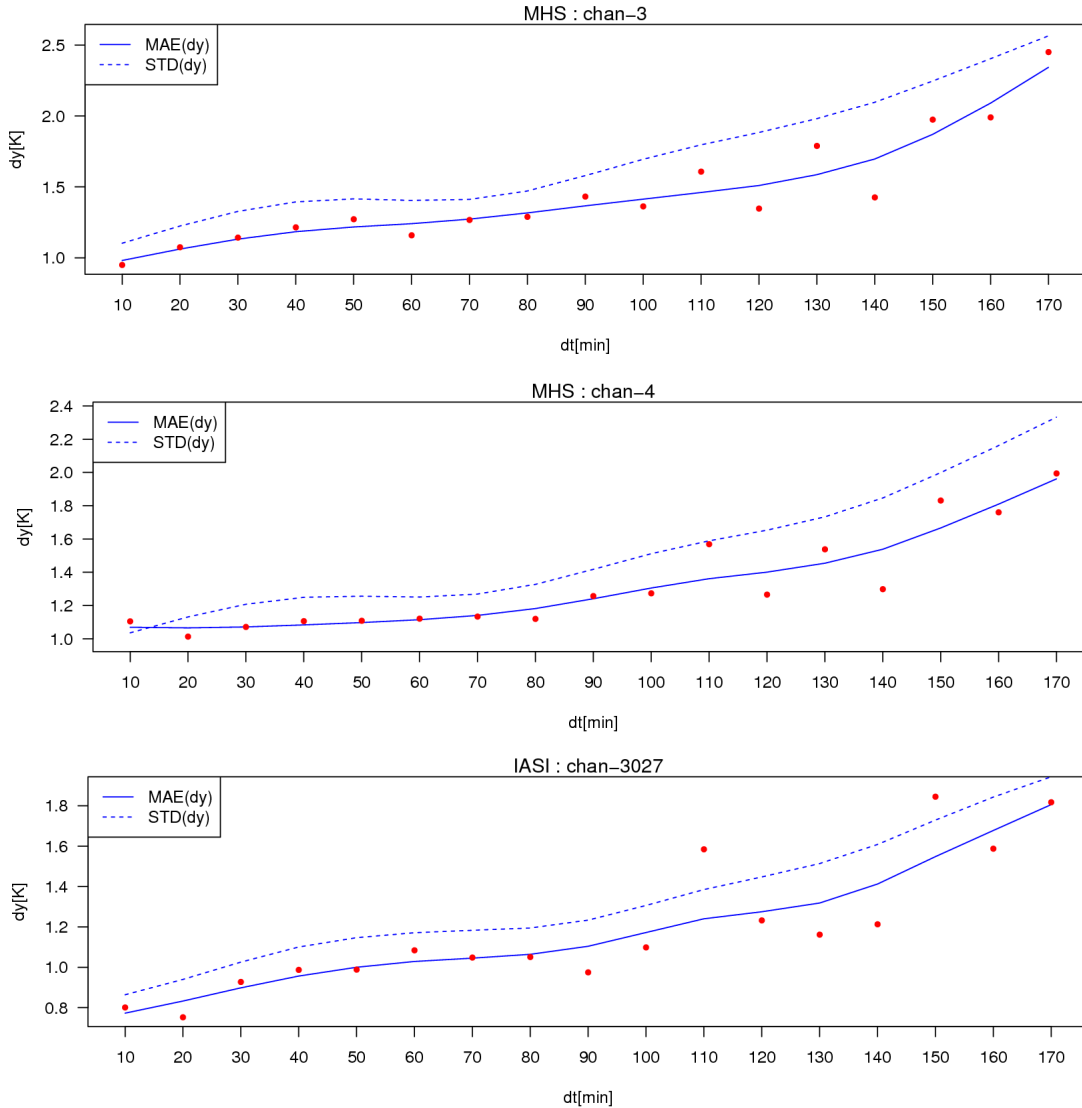


Figure 15: Dependency of observation increments  $\delta y$  on time-delay  $\delta t$  for middle-tropospheric humidity channel-3, 4 (MHS) and channel-3027 (IASI).

The effect of time-delay on observation increment error is shown for MRH channels in Fig 15. There is a mean absolute error (MAE) and standard deviation (STD) of observation increments  $\delta y$  depending on time-delays  $\delta t$  for sensor MHS/channel-3, 4 and IASI/channel-3027. It is obvious that increasing time-delay leads to increasing STD as well as MAE of increments. Note that the increment

error on the edge of assimilation window ( $\delta t = 180$  min) is two-times bigger then in the center of window close to analysis time ( $\delta t = 10$  min).

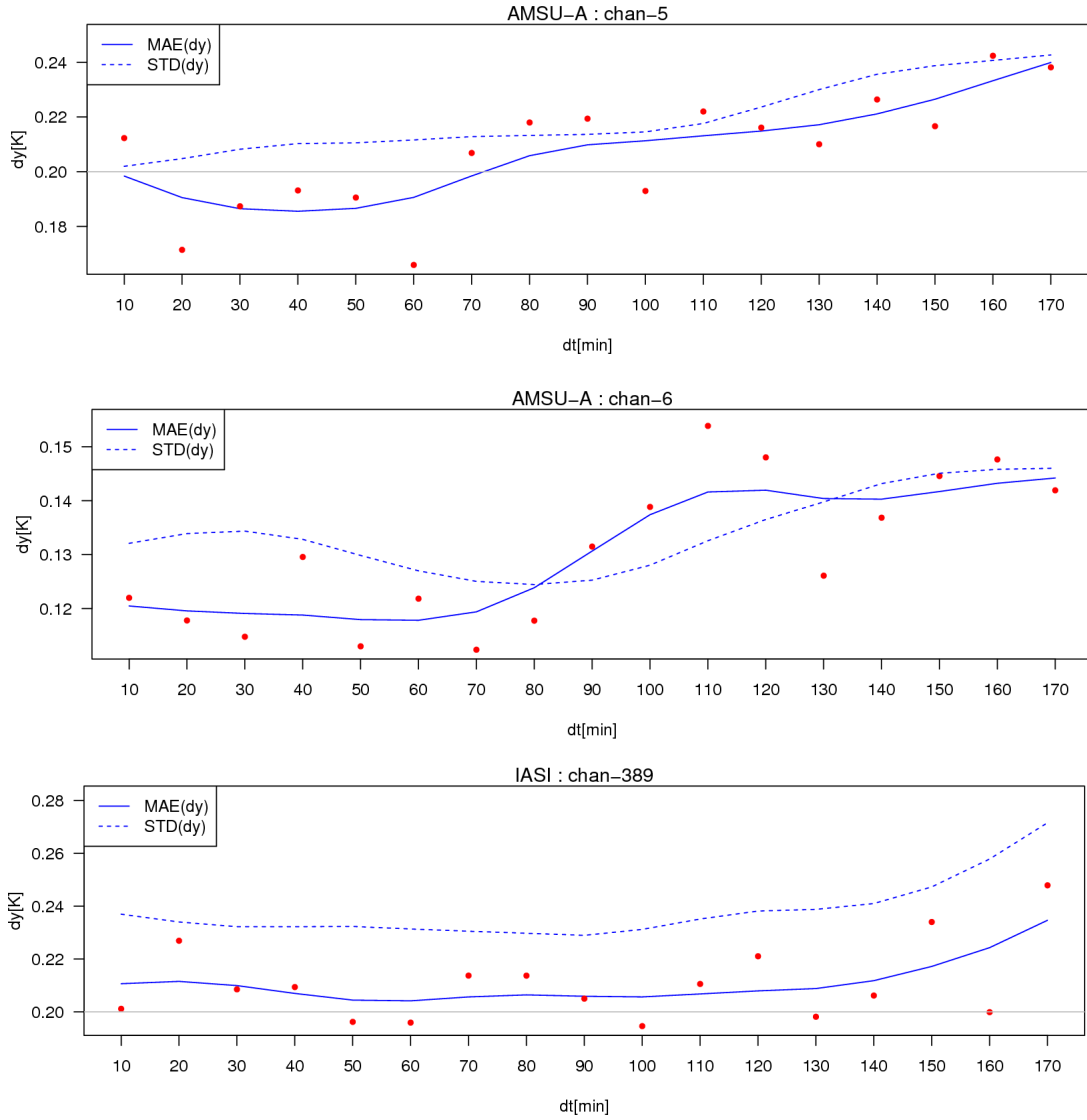


Figure 16: Dependency of observation increments  $\delta y$  on time-delay  $\delta t$  for low-tropospheric temperature channel-5, 6 (AMSU-A) and channel-389 (IASI).

The effect of time-delay is shown for LT and MT channels in Fig 16. There are increment error statistics for sensor AMSU-A/channel-5, 6 and IASI/channel-389. Note that there is an increasing dependence between the increments error and time-delays for sensor AMSU-A, whereas this dependency is reduced for the IASI sensor due to the cloud-detection scheme (see Sec 3.3). We detected increasing bias for observation delayed:

- more than 1 hour from analysis for LT channel-5 (peaking around 1000 – 500 hPa)
- more than 1.5 hour from analysis for MT channel-6 (peaking around 500 – 300 hPa)

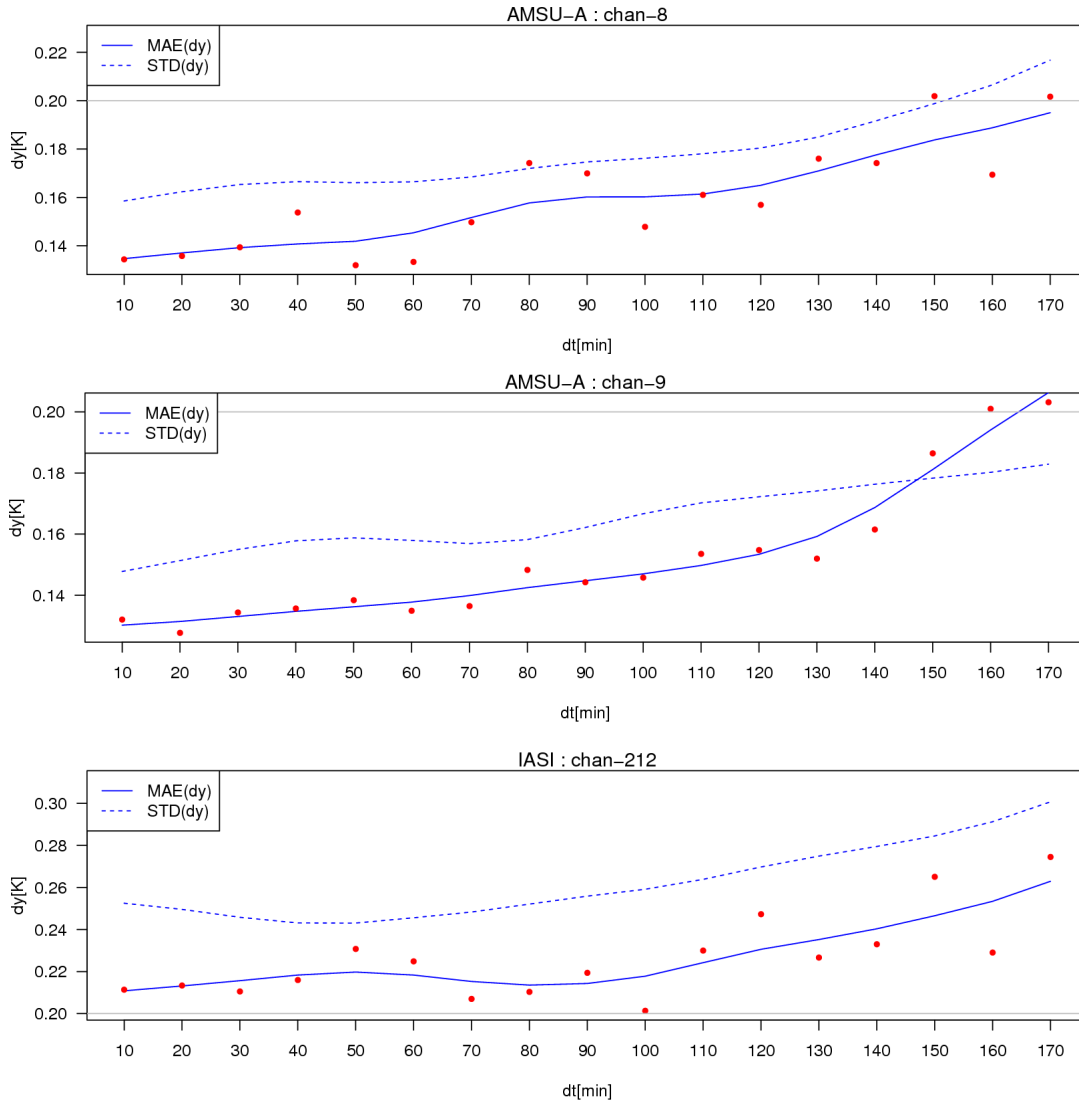


Figure 17: Dependency of observation increments  $\delta y$  on time-delay  $\delta t$  for high-tropospheric temperature channel-8, 9 (AMSU-A) and channel-219 (IASI).

Finally we detect an increasing dependence also for HT channels. The stronger dependence is monitored for sensor AMSU-A and the reduced dependence for sensor IASI shown in Fig 17. Note that the detected bias increases slightly for time-delay more then 1 hour (channel-8) and more significantly for time-delay more then 2 hours (channel-9).

## 4 Conclusion

The aim of this report is finding an effect of time-delay between observation and analysis time in case of non-stationary weather conditions. We assess polar satellites measurements providing information about atmospheric temperature and humidity. This data are provided not in analysis time, but within an assimilation window including data  $\pm 3h$  around the analysis time.

We examined time-delays of polar satellites crossing our model domain in Sec 3.1. We have available data from the polar satellites NOAA-18, 19 and MetOp-A, B. The satellites crossing times are shown in Fig 3 and their mean time-delays are described in Tab 1. In summary, the polar satellites provide measurements over the ALADIN/CZ domain time-delayed above 2 – 3 hours from analysis time except of polar satellite NOAA-19 sensing the domain near analysis time (up to 1-hour delayed).

We study an effect of a non-stationary weather conditions in combination with time-delay on:

1. temperature- and humidity-sensitive sensors
2. satellite channels providing information at different altitudes
3. a cloud-detection scheme specific to sensor IASI

The studied channel selection is described in Tab 2. There are temperature-sensitive channels peaking in high- (HT), middle- (MT), low-troposphere (LT) channels, the surface (ST) channels and humidity channels peaking in middle-troposphere (MRH). The effect of non-stationary weather conditions (from 3.9.2013) on observation increment is studied for the two time-delays  $\delta t_1 = 20min$  and  $\delta t_2 = 160min$ . We found out that the effect of the time-delay increases for the non-stationary weather conditions related with an extra-tropical cyclone e.g. cold/warm front lines, a warm/cold advection or a cloud-effect. This is shown in smoothed observation increment fields providing observation-minus-guess departures. The increasing increments are more significant for MRH channels shown in Fig 7 then for temperature-sensitive channels. This is due to strong gradient of humidity near the cold/warm front affected moreover by clouds.

The temperature-sensitive channels were affected less then MRH channels, however, a significant increasing of observation increments was detected for HT, LT and ST channels. The HT channels are affected due to the non-stationary cold/warm advection above 200 – 300hPa shown for AMSU-A/channel 8 in Fig 9. The LT/ST channels are affected due to the non-stationary surface temperature varying with regards to the solar insolation during a day. This effect manifesting by increasing observation increments is shown for sensor AMSU-A/channel 5 in Fig 10.

The cloud detection scheme (McNally and Watts 2003) is applied for IASI measurements to avoid a contamination by cloudy-radiances not exactly assimilated in the current system. The effect of time-delay on the scheme quality is studied in non-stationary conditions. We found out that the scheme works optimally supposing unbiased observation and model guess. The increasing time-delay leads to increasing observation increments affecting cloud-type detection and degrade the quality of cloudy-channel rejection. This effect is shown for IASI-MRH/channel-3027 in Fig 12 and IASI-HT/channel-219 in Fig 14, where are the selected clear-sky radiances compared with CMS cloud-type product. The increasing observation increments due to time-delay are assessed as cloudy-pixels and incorrectly rejected. This leads to reduction of the time-delay effect and reduction of observation increment errors.

The effect of time-delay on polar satellite instruments/channels is assessed for a long-time period assessed in Tab 3, Tab 4 and Tab 5. The long time statistics (BIAS, STD) confirm the before mentioned results from the non-stationary case study.

In addition, we found out that the time-delay could affect a quality of bias correction with regards to input bias parameters. The parameters used from global model are not able to represent the increasing BIAS value for ST and LT channels and it leads to a bias degradation. However, the parameters cycled in LAM are able to adapt to increasing BIAS value and it leads to the better bias correction (not shown in this report).

Finally, we study a dependence between different time-delays and observation increments to find an optimal length of assimilation window. The stronger dependences were found for sensors AMSU-A and MHS and channels MRH, LT and HT as is shown in Fig 15, Fig 16 and Fig 17. For sensor IASI was detected the effect of cloud-detection scheme that reduce the time-delay problem in observation increments.

The optimal length of assimilation window could be found as a compromise between a sample of polar satellite observation and error due to time-delay. Taking into account the satellite coverage over the domain (primarily 2 – 3 hours from analysis time) and the dependency of observation increments error on time-delays (for MRH, HT, LT and ST channels), we suggest 3h-assimilation window as the optimal length for polar satellite data assimilation.

To conclude the assumption of stationary model field within the 6h-assimilation window is not fulfill for non-stationary weather situation e.g within extra-tropical cyclones. This problem leads to increasing error of observation increments that could degrade analysis and forecast. The assimilation window reduction from 6-hours to 3-hours should lead to improvement of polar-satellite data assimilation, however, we reject about half of observation outside the window. To avoid this rejection problem there are another options how to analyzed the observations:

- The 3h-RUC (Rapid Update Cycling) – has benefit from higher frequency of assimilation cycle up to a three-hour forward intermittent cycle. Then the 3h-assimilation window could cover all available observations during a day.
- The 3D-FGAT (First Guess at Appropriate Time) – observation increments are computed at the right observation time, however, this increment is not propagated back and forth in time by a model (approximation of 4D-Var). We could preserve 6h-assimilation window, in spite of the time-delay problem.

These two methods appear to be an attractive compromise between accuracy and overall computing time and will be further investigated.

## A Cloud detection scheme

The technique of this scheme is shown in Fig 18. In summary, this cloud detection algorithm works by taking the observation increments (marked as BT departure) and looking for the signature of opacity that is not included in the clear-sky calculation. To do this, at first the channels are ordered according to their height assignment with the highest channels first and the channels closest to the surface last (x-axis in figure). The sorted increments are then smoothed with a moving-average filter in order to reduce the effect of instrument noise.

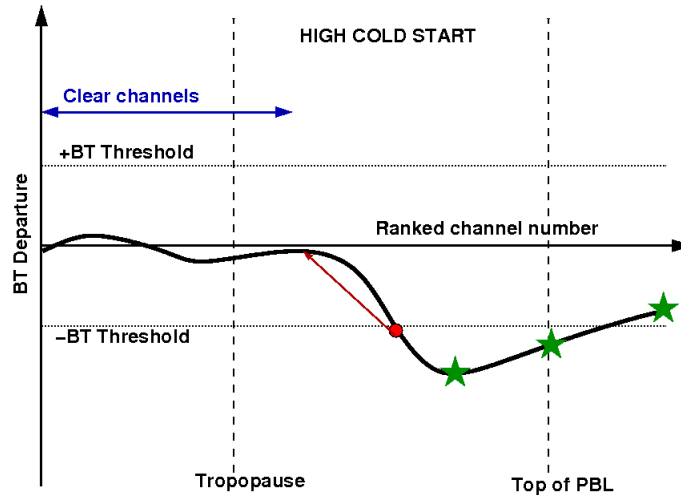


Figure 18: The cloud detection scheme to reject cloudy channels for sensor IASI described by McNally et al (2003). The source is [www.nwpsaf.eu](http://www.nwpsaf.eu).

Presence of the cloud-effect is judged on the basis of FG departure check and window-gradient check. In the FG departure check, the smoothed FG departure is compared with a threshold value (BT threshold is 0.5 K). In the window-gradient check, gradient of the smoothed FG departure within the long-wave window channels is compared with another threshold value. If no cloud radiative effect is found in either one of these checks, the sounding is flagged completely clear of clouds. For more details see [8].

## References

- [1] Berre, L., tefnescu S., and Pereira B.P, 2006: **The representation of analysis effect in three error simulation techniques.** Tellus, Ser. A, 58, 196209
- [2] Brozkova, R., and Coauthors, 2001: **DFI blending, an alternative tool for preparation of the initial conditions for LAM.** PWRP Rep. 31 (CAS/JSC WGNE Rep.), WMO-TD-1064, 1-7.
- [3] Chambers J M, Hastie T J, 1992: **Statistical Models in S.** Wadsworth & BrooksCole.
- [4] Chevallier F, Di Michele S, McNally A., 2006: **Diverse profile datasets from the ECMWF 91-level short-range forecasts** NWP SAF report NWPSAF-EC-TR-010. EUMETSAT: Darmstadt, Germany.
- [5] Gandin, L. S., 1963: **Objective analysis of meteorological fields** Gidrometeorologicheskoe Izdatelstvo, Leningrad. English translation by Israeli Program for Scientific Translations, Jerusalem, 1965.

- [6] *Lorenc, A. C., 1997: Development of an operational variational assimilation scheme.* J. Meteorol. Soc. Jpn.,75(1B), 339346
- [7] *Panguaud T, Fourrie N, Guidard V, Dahoui M, RAabier F, 2009: Assimilation of AIRS radiances affected by mid to low level clouds.* Mon. Weather Rev. 137:4276-4292.DOI:10.1175/2009MWR3020.1.
- [8] *McNally AP., Watts PD., 2003: A cloud detection algorithm for high-spectral-resolution infrared sounders.* Q.J.R. Meteorol. Soc. 129:3411-3423
- [9] *2012: Product User Manual for 'Cloud Products' (CMa-PGE01 v3.2, CTPGE02 v2.2 & CTTH-PGE03 v2.2), Issue 3, Rev. 2*